On slow manifolds of chemically reactive systems

Sandeep Singh,[a] Joseph M. Powers,[b] and Samuel Paolucci[c]
Department of Aerospace and Mechanical Engineering, University of Notre Dame, Notre Dame, Indiana 46556-5637

(Received 13 November 2001; accepted 23 April 2002)

This work addresses the construction of slow manifolds for chemically reactive flows. This construction relies on the same decomposition of a local eigensystem that is used in formation of what are known as Intrinsic Low Dimensional Manifolds (ILDMs). We first clarify the accuracy of the standard ILDM approximation to the set of ordinary differential equations which model spatially homogeneous reactive systems. It is shown that the ILDM is actually only an approximation of the more fundamental Slow Invariant Manifold (SIM) for the same system. Subsequently, we give an improved extension of the standard ILDM method to systems where reaction couples with convection and diffusion. Reduced model equations are obtained by equilibrating the fast dynamics of a closely coupled reaction/convection/diffusion system and resolving only the slow dynamics of the same system in order to reduce computational costs, while maintaining a desired level of accuracy. The improvement is realized through formulation of an elliptic system of partial differential equations which describe the infinite-dimensional Approximate Slow Invariant Manifold (ASIM) for the reactive flow system. This is demonstrated on a simple reaction-diffusion system, where we show that the error incurred when using the ASIM is less than that incurred by use of the Maas-Pope Projection (MPP) of the diffusion effects onto the ILDM. This comparison is further done for ozone decomposition in a premixed laminar flame where an error analysis shows a similar trend. [DOI: 10.1063/1.1485959]

I. INTRODUCTION

A wide variety of combustion processes involve a large number of elementary reactions occurring simultaneously within a complex flow field. These processes are modeled by a large number of partial differential equations (PDEs) representing the evolution of numerous reactive chemical species, coupled with the full Navier–Stokes equations. Fully resolved solution of these model equations, which incorporate detailed finite rate chemical kinetics, often requires a prohibitive amount of computational resources. Hence, there is a need to develop methods which rationally reduce the model equations such that numerical simulations can be accomplished in a reasonable amount of computational time. Elementary chemical reactions occur over a wide range of time scales which is manifested as stiffness in the model equations, and subsequently high computational costs. For stable systems, this stiffness can be reduced by systematically equilibrating the fast time scale chemical processes and resolving only the relevant slow time scale chemical processes. The reduced model equations describe the slow dynamics under the assumption that the fast dynamics can be neglected. Most chemical time scales are faster than time scales associated with fluid mechanical phenomenon such as convection and diffusion. Nevertheless, it is important that the reduced model equations maintain the coupling of the flow processes with those chemical processes which occur at similar time scales. In this work we illustrate how this coupling of fluid and chemical processes can be maintained such that an approximate and less expensive numerical solution of the reduced model equations is consistent with the more accurate and expensive numerical solution of the full model equations.

Several strategies have been used for reduction of detailed chemical kinetics. The simplest method of frozen flow assumes all chemical species to have fixed mass fractions. Another approach assumes all chemical species to be in full equilibrium, which is equivalent to the assumption that all chemical processes occur at an infinitely fast time scale. These approaches, discussed by Vincenti and Kruger,[1] miss the coupling between chemical processes and flow events which occur at similar finite time scales. Simple and often useful strategies, which may capture some of the reaction time scales, consist of systematically replacing hundreds of elementary reaction steps by explicit one- or two-step reaction models.[2–5] Also useful are the commonly employed partial equilibrium assumptions for some of the elementary reactions, and steady state assumptions for some of the chemical species.[6,7] However, these methods require substantial, fallible intuition, and considerable human time to develop. Another problem with these approaches is that while the reduced models may be useful for a certain range of compositions of chemical species for which they have been calibrated, it is often easy to find scenarios where they cannot accurately reproduce the results of full chemical kinetics.[8] Other approaches for obtaining reduced chemical kinetics models include lumping methods,[9] sensitivity analysis,[10] and optimization approaches.[11,12] The review ar-

[a]Ph.D. candidate. Electronic mail: ssingh@nd.edu
[b]Associate Professor. Electronic mail: powers@nd.edu
[c]Professor. Electronic mail: paolucci@nd.edu

ticles by Griffiths[13] and Okino *et al.*[14] discuss in detail most of these reduction strategies.

The methods of Intrinsic Low Dimensional manifolds (ILDM) (Ref. 8) and Computational Singular Perturbation (CSP) (Refs. 15,16) use a dynamical systems approach of time scale analysis to systematically reduce the stiffness introduced by chemistry. Both methods are developed for spatially homogeneous premixed reactive systems (in the absence of any transport processes such as convection and diffusion), which can be modeled by systems of ordinary differential equations (ODEs). The behavior of these reactive systems can be described by trajectories in the associated phase space or composition space starting from an initial condition and relaxing to a chemical equilibrium.

The ILDM method identifies *ab initio* a low-dimensional subspace, known as the ILDM, within the composition space, which closely approximates the subspace in which slow time scale processes evolve. For systems initially off the ILDM, all the fast processes rapidly approach the ILDM and partially equilibrate. If n chemical species are involved in the chemical kinetics scheme, then in the n-dimensional composition space, an m-dimensional ($m<n$) ILDM can be identified by a local eigenvalue-eigenvector analysis. If the chemical processes associated with $(n-m)$ fast time scales are equilibrated, then the chemical processes associated with m slow time scales occur close to the m-dimensional ILDM in the composition space. On the m-dimensional ILDM, m ODEs with reduced stiffness are required to be solved coupled with $(n-m)$ nonlinear algebraic equations describing the ILDM. The ILDM method is only useful after the phase space trajectory which starts from the initial condition has relaxed onto the ILDM. This is acceptable under the assumption that fast time scale processes can be neglected. A proper projection is required from the initial condition to the ILDM such that there is at most a small temporal phase error between the solution obtained using the ILDM method and the solution of the full system of ODEs.

The CSP method also uses a local eigenvalue-eigenvector analysis to reduce the stiffness, but does not reduce the number of dependent variables.[17] Another advantage of the ILDM method is that the ILDM can be computed *a priori* in the composition space and stored in a table. Hence, the ILDM method has a significant computational advantage over the CSP method, as the expensive computation of local eigenvalues and eigenvectors is not required during the actual computations with the reduced model equations. A number of studies have appeared in recent years advancing the ILDM method and some variants, cf. Blasenbrey *et al.*,[18] Eggels *et al.*,[19] Schmidt *et al.*,[20] Yang *et al.*,[21] Rhodes *et al.*,[22] Lowe *et al.*,[23] Gicquel *et al.*,[24] and Correa *et al.*[25]

The ILDM is only an approximation of what we call the Slow Invariant Manifold (SIM). Relative to the more fundamental SIM, the ILDM contains a small intrinsic error for large finite stiffness. Consequently, it will be shown that the contention of Rhodes *et al.*[22] that the Maas and Pope algorithm identifies a slow invariant manifold is in error. The SIM, which can be obtained analytically by perturbation analysis[26] for simple systems, or using algebraic functional iteration[27,28] or computed using numerical functional iteration[29] for more complex systems, describes the slow dynamics of the spatially homogeneous reactive systems accurately. However, provided that a spectral gap condition is satisfied, the ILDM does a good job of approximating the SIM, and in our experience, computation of high dimensional ILDMs appears to be more tractable than that of high dimensional SIMs.

The previously described methods achieve computational efficiency in spatially homogeneous reactive systems modeled by a system of ODEs. In more realistic problems it is important to achieve similar computational efficiency for simulating spatially inhomogeneous reactive systems which are modeled by PDEs and which have infinite dimensional SIMs. Hadjinicolaou *et al.*[30] have extended the CSP method to reaction diffusion equations. Yannacopolous *et al.*[31] illustrate, using inertial manifolds, infinite dimensionality of slow manifolds associated with PDEs when compared to finite dimensionality of slow manifolds associated with ODEs. However, the algebraic determination of these infinite-dimensional inertial manifolds is only suitable for simpler cases where the segregation of slow and fast variables is fixed for all times and throughout phase space. This is not the case with general systems of chemical kinetics where compositions of slow and fast variables change locally in phase space.

Maas and Pope have proposed an extension of the ILDM method to reactive flow systems described by PDEs.[32] They assume that if flow processes occur at time scales of the order of the m slow chemical time scales associated with the m-dimensional reaction ILDM, then the flow processes only perturb the system off the ILDM, while the fast chemical processes rapidly relax the system back onto the ILDM. Therefore, in the Maas and Pope Projection (MPP), convection-diffusion terms in reactive flow PDEs are projected back onto the finite dimensional tangent subspace of the ILDM, signifying that the reactive system never leaves the ILDM in the composition space. The dimension of the ILDM to be used is determined by prescribing a cutoff for the chemical time scales, based on the fastest flow time scales. If the flow time scales are faster than the chemical time scales associated with an ILDM of a certain dimension, then a higher dimensional ILDM is required, which is essential to maintain full coupling of the flow and chemical processes. A problem with the MPP method is that a different dimensional ILDM is often required at different locations in physical space as the flow time scales vary locally and the chemical time scales vary in both physical and composition spaces. Hence, this amounts to solving a different number of reduced PDEs at different locations in physical space. Another problem is that it is difficult to determine *a priori* the magnitude of the flow time scales which control the dimension of the ILDM to be used.

One way to overcome these problems is to use Strang operator splitting[33] between the reaction source terms and the convection-diffusion terms when solving the reactive flow model equations.[34] In the first step, each point in physical space is treated as a spatially homogeneous premixed reactor with convection-diffusion suppressed, and the resulting

ODEs for the reaction part are solved using the standard ILDM method. This allows the use of different dimensions of the ILDM at different locations in physical space. If the chemical composition at a certain location in the physical space does not lie near the ILDM, implicit integration of the full equations is used in the reaction step, until the chemical composition relaxes to the ILDM. In the second step, the reaction part of the reactive flow equations is suppressed, and the resulting PDEs for the convection-diffusion part are solved using standard discretization techniques for inert flows. The second step perturbs the reactive system off the ILDM; it is projected back onto the ILDM along the direction of the fast eigenvectors associated with the chemistry in the composition space. Even though the ILDM method reduces the number of ODEs to be solved in the first step, the number of PDEs to be solved in the second step is the same as the number of original model equations. Another disadvantage of this method is that errors are incurred due to operator splitting. Strang splitting has second order accuracy in time provided both steps have second order accuracy. If the chemical time scales are highly disparate from the flow times scales, the operator splitting method will induce errors in wave speeds. These can be minimized by resolving the spatial and temporal scales in the thin reaction zones using adaptive mesh refinement methods.[35]

In this work we propose a more systematic approach to preserve the coupling between chemistry and flow physics. The full model equations are projected onto the fast and slow basis vectors associated with chemistry. A set of elliptic PDEs is obtained by equilibrating the fast dynamics. These elliptic PDEs are analogous to the algebraic equations describing the ILDM. The elliptic PDEs describe the infinite-dimensional Approximate Slow Invariant Manifold (ASIM) to which the reactive flow system relaxes to before reaching steady state. The ASIM accounts for the effects of convection and diffusion in the reactive flow system, as opposed to the ILDM. When using the ASIM, we solve a set of elliptic PDEs in physical space coupled with time-dependent reduced PDEs associated with the slow dynamics.

The paper is organized as follows. A description of the standard ILDM method developed for a spatially homogeneous premixed reactor is first given. It is then shown that the ILDM is an approximation of the SIM for a spatially homogeneous reactive system. Then a theoretical development of the ASIM associated with a spatially inhomogeneous reactive system, as an extension for the standard ILDM method, is discussed. Subsequently, we compare and contrast use of the ASIM with that of the MPP method for a simple reaction diffusion model problem. Finally, a similar comparison is also made for the decomposition of ozone in a one-dimensional premixed laminar flame.

II. ILDM METHOD FOR A SPATIALLY HOMOGENEOUS PREMIXED REACTOR

A spatially homogeneous premixed reactor can be modeled by the system of ODEs,

$$\frac{d\mathbf{y}}{dt}=\mathbf{f}(\mathbf{y}), \quad \mathbf{f}(\mathbf{0})=\mathbf{0}, \tag{2.1}$$

where $\mathbf{y}\in\mathcal{R}^n$ represents a set of dependent variables, $\mathbf{f}(\mathbf{y})$ is the reaction source term typically modeled by Arrhenius chemical kinetics, and t is the independent time variable. Without loss of generality, the origin is translated to the chemical equilibrium point, which, for fixed mass adiabatic systems, has a unique value when the domain is restricted to physically accessible regions of composition space.[36] The nonlinear reaction source term typically induces severe stiffness in Eq. (2.1) and makes it computationally expensive to solve. The stiffness is due to the widely disparate time scales over which different chemical reactions occur. The eigenvalues of the Jacobian $\mathbf{J}=\partial\mathbf{f}/\partial\mathbf{y}$ identify the local time scales associated with the reactive system. The eigenvectors of $\mathbf{J}$ identify the local directions associated with the corresponding time scales in the n-dimensional phase space. It is ensured that there are no zero eigenvalues by eliminating all conserved quantities from Eq. (2.1). These conserved quantities can arise, for example, due to the conservation of atoms in the spatially homogeneous premixed reactor, and can be described by algebraic equations. The eigenvalues and eigenvectors can be obtained by the following decomposition of $\mathbf{J}$, with $\tilde{\mathbf{V}}=\mathbf{V}^{-1}$:

$$\mathbf{J}=\mathbf{V}\mathbf{\Lambda}\tilde{\mathbf{V}}, \tag{2.2a}$$

$$\mathbf{V}=\begin{pmatrix} | & & | & | & & | \\ \mathbf{v}_1 & \cdots & \mathbf{v}_m & \mathbf{v}_{m+1} & \cdots & \mathbf{v}_n \\ | & & | & | & & | \end{pmatrix}=(\mathbf{V}_s \vdots \mathbf{V}_f), \tag{2.2b}$$

$$\mathbf{\Lambda}=\begin{pmatrix} \lambda_{(1)} & & 0 & \vdots & & \\ & \ddots & & & 0 & \\ 0 & & \lambda_{(m)} & \vdots & & \\ \cdots & \cdots & \cdots & \cdots & \cdots & \cdots \\ & & & \lambda_{(m+1)} & & 0 \\ & 0 & & & \ddots & \\ & & & 0 & & \lambda_{(n)} \end{pmatrix}$$
$$=\begin{pmatrix} \mathbf{\Lambda}_{(s)} & \vdots & 0 \\ \cdots & \vdots & \cdots \\ 0 & \vdots & \mathbf{\Lambda}_{(f)} \end{pmatrix}, \tag{2.2c}$$

$$\tilde{\mathbf{V}}=\begin{pmatrix} - & \tilde{\mathbf{v}}_1 & - \\ & \vdots & \\ - & \tilde{\mathbf{v}}_m & - \\ \cdots & \cdots & \cdots \\ - & \tilde{\mathbf{v}}_{m+1} & - \\ & \vdots & \\ - & \tilde{\mathbf{v}}_n & - \end{pmatrix}=\begin{pmatrix} \tilde{\mathbf{V}}_s \\ \cdots \\ \tilde{\mathbf{V}}_f \end{pmatrix}. \tag{2.2d}$$

Here $\mathbf{v}_1,\ldots,\mathbf{v}_n$ represent the right eigenvectors of $\mathbf{J}$ and form the column vectors of the $n\times n$ right eigenvector matrix $\mathbf{V}$. The diagonal matrix $\mathbf{\Lambda}$, also of dimension $n\times n$, contains the eigenvalues, $\lambda_{(1)},\ldots,\lambda_{(n)}$, of $\mathbf{J}$ along its main diagonal, with their real parts ordered from least negative to most negative. Sufficiently close to the chemical equilibrium point, all the eigenvalues are real and negative. Thus, for the following discussion, we will assume that all eigenvalues are real and negative. The reciprocal vectors to the right eigenvectors are represented by $\tilde{\mathbf{v}}_1,\ldots,\tilde{\mathbf{v}}_n$, which form the row

vectors of the inverse right eigenvector matrix $\tilde{\mathbf{V}}$. The local time scales in phase space are given by the inverse of the magnitudes of the eigenvalues, $1/|\lambda_{(1)}|, \ldots, 1/|\lambda_{(n)}|$, and are ordered from slowest to fastest.

Defining $\mathbf{g}$ to be the nonlinear part of $\mathbf{f}$,

$$\mathbf{g}=\mathbf{f}-\mathbf{J}\mathbf{y}, \tag{2.3}$$

Eq. (2.1) can be rewritten as

$$\frac{d\mathbf{y}}{dt}=\mathbf{J}\mathbf{y}+\mathbf{g}. \tag{2.4}$$

A new set of variables defined by $\mathbf{z}=\tilde{\mathbf{V}}\mathbf{y}$ is used with Eq. (2.4) to obtain

$$\frac{d\mathbf{z}}{dt}+\tilde{\mathbf{V}}\frac{d\mathbf{V}}{dt}\mathbf{z}=\mathbf{\Lambda}\mathbf{z}+\tilde{\mathbf{V}}\mathbf{g}. \tag{2.5}$$

The time evolution of processes associated with the i-th time scale, in Einstein notation, is given by

$$\frac{1}{\lambda_{(i)}}\left(\frac{dz_i}{dt}+\tilde{\mathbf{v}}_i\sum_{j=1}^{n}\frac{d\mathbf{v}_j}{dt}z_j\right)=z_i+\frac{1}{\lambda_{(i)}}(\tilde{\mathbf{v}}_i\mathbf{g}),\quad i=1,\ldots,n. \tag{2.6}$$

It is assumed that we are not interested in the dynamics of events which occur at a time scale of $1/|\lambda_{(m+1)}|$ or faster, and that there are m slow time scales and $(n-m)$ fast time scales.

The transients of fast processes equilibrate before transients of the slow processes because the fast processes are associated with the eigenvalues which are negative and large in magnitude. Equation (2.6) represents the dynamical system in Eq. (2.1), in a form equivalent to that of a singularly perturbed system,[37] with $1/|\lambda_{(m+1)}|, \ldots, 1/|\lambda_{(n)}|$ as the small parameters multiplying the time derivatives on the left-hand side of the equations. Hence, by neglecting the left-hand side of Eq. (2.6) for $i=m+1,\ldots,n$, we effectively equilibrate the fast dynamics and obtain a set of approximate $(n-m)$ algebraic equations given by

$$z_i+\frac{1}{\lambda_{(i)}}(\tilde{\mathbf{v}}_i\mathbf{g})=0,\quad i=m+1,\ldots,n. \tag{2.7}$$

This is expected to be accurate only if a significant spectral gap exists between $|\lambda_{(m)}|$ and $|\lambda_{(m+1)}|$. A direct substitution of Eqs. (2.2), (2.3), and the definition of $\mathbf{z}$ is used to rewrite Eq. (2.7) as

$$\tilde{\mathbf{V}}_f\mathbf{f}=\mathbf{0}, \tag{2.8}$$

which is the algebraic equation for the ILDM as obtained by Maas and Pope.[8] The matrix $\tilde{\mathbf{V}}_f$ has dimension $(n-m)\times n$, and its row vectors contain the reciprocal vectors of the right eigenvectors associated with the $(n-m)$ fast time scales. In writing Eq. (2.7), we are assuming that $\|\mathbf{g}\|=\mathcal{O}(|\lambda_{(m+1)}|)$ or greater, and hence, the second term cannot be neglected. The ILDM is an approximation of an m-dimensional subspace, defined by Eq. (2.8), within an n-dimensional phase space on which processes associated with slow time scales occur. The fast time scale processes, prior to equilibration, rapidly approach the ILDM. Once the fast time scale processes have equilibrated, the slow dynamics for Eq. (2.1) can be approximated by what we refer to as the standard ILDM method, which is defined by the following set of differential algebraic equations,

$$\tilde{\mathbf{V}}_s\frac{d\mathbf{y}}{dt}=\tilde{\mathbf{V}}_s\mathbf{f}, \tag{2.9a}$$

$$\mathbf{0}=\tilde{\mathbf{V}}_f\mathbf{f}, \tag{2.9b}$$

where the matrix $\tilde{\mathbf{V}}_s$ has dimension $m\times n$, and its row vectors contain the reciprocal vectors to the right eigenvectors associated with the m slow time scales.

The differential algebraic Eqs. (2.9) have reduced stiffness compared to the original Eq. (2.1), and the number of ODEs to be integrated has also been reduced to m. The reduction in stiffness allows for larger time steps when integrating Eqs. (2.9), than when integrating the original Eq. (2.1) with explicit numerical methods, thereby reducing the computational time. Moreover, because matrix inversions are not necessary, the method is faster than implicit methods as well. To further reduce computational time, the algebraic Eq. (2.9b) is solved *a priori* in a predetermined domain of the n-dimensional phase space. The m-dimensional ILDM in phase space, obtained by the solution of the Eq. (2.9b), is stored in a table parameterized by m chosen state variables. The table can then be used during the integration of Eq. (2.9a), instead of solving the differential algebraic system of Eqs. (2.9). Another advantage of storing the ILDM in tabular form is that the table can be re-used for different sets of computations involving the same reaction kinetics. Details of this procedure and the computation of the ILDM in phase space is given by Maas.[38]

Outside the subspace of the m-dimensional ILDM, Eqs. (2.9) do not apply. In general, initial conditions may not lie on the ILDM, though the trajectory starting from an arbitrary initial condition in the phase space will rapidly approach the ILDM as the fast time scale processes equilibrate. The projection of the initial condition onto the ILDM has to be done carefully in order to avoid a large phase error in the time-dependent solution of the reduced differential algebraic system of equations. An accurate method, although computationally expensive, is to use implicit integration of the full system of Eq. (2.1), until the trajectory is close to the ILDM, and then integrate the reduced differential algebraic system of equations.[34] A more efficient approach remains an outstanding problem.

Based on Eq. (2.8), the ILDM can also be defined as an m-dimensional subspace of the n-dimensional phase space where the vector $\mathbf{f}$ lies in the local linear subspace spanned by the eigenvectors associated with the slow time scales. This is illustrated in Fig. 1 for a two-dimensional system. For $n=2$, $\mathbf{V}_s=\mathbf{v}_1$ and $\mathbf{V}_f=\mathbf{v}_2$ are the eigenvectors associated with slow and fast time scales, respectively. The corresponding reciprocal bases, are given by the vectors $\tilde{\mathbf{V}}_s=\tilde{\mathbf{v}}_1$ and $\tilde{\mathbf{V}}_f=\tilde{\mathbf{v}}_2$. Figure 1 also gives a graphical representation of Eq. (2.8) describing the ILDM. The ILDM consists of the set of points in phase space where the vector $\mathbf{f}$ has the same orientation as the slow eigenvector $\mathbf{V}_s$. This does not ensure that

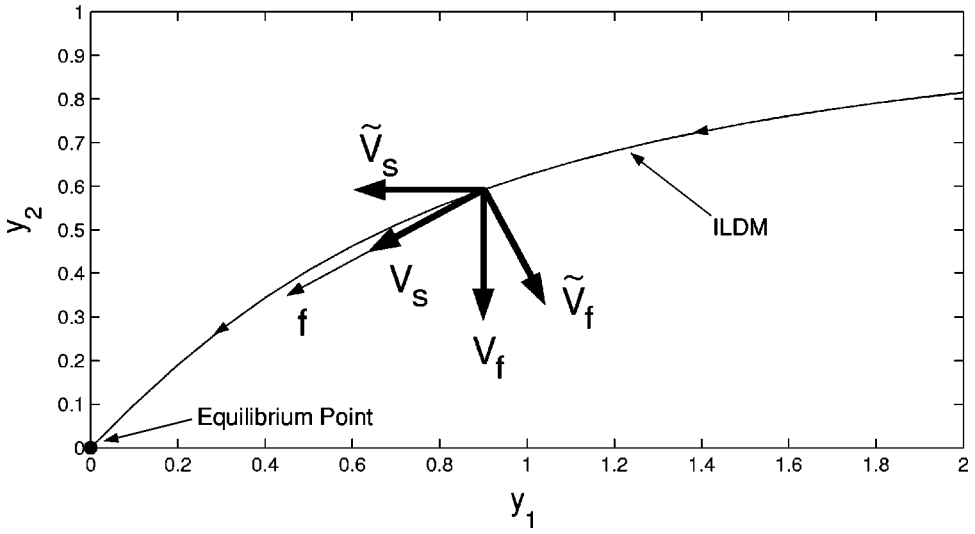

FIG. 1. Graphical representation of the ILDM for a two-dimensional dynamical system, depicting that the ILDM is a set of points in the phase space where the vector $\mathbf{V}_s$ has the same orientation as the vector $\mathbf{f}$.

the vector $\mathbf{f}$ is tangent to the ILDM. By definition[37] an invariant manifold is a subspace $S \subset \mathcal{R}^n$, if for any solution $\mathbf{y}(t)$, $\mathbf{y}(0) \in S$, of Eq. (2.1), implies that for some $T>0$, $\mathbf{y}(t) \in S$ for all $t \in [0,T]$. Hence, the SIM, like all invariant manifolds, is also a trajectory in phase space, and the vector $\mathbf{f}$ must be tangent to it.

It is easily shown that the ILDM is not a trajectory in phase space; instead, it is only an approximation of the SIM. Using Eq. (2.8), the normal vector to the ILDM is given by

$$\nabla(\tilde{\mathbf{V}}_f \mathbf{f}) = \tilde{\mathbf{V}}_f \mathbf{J} + (\nabla \tilde{\mathbf{V}}_f)\mathbf{f} = \mathbf{\Lambda}_{(f)} \tilde{\mathbf{V}}_f + (\nabla \tilde{\mathbf{V}}_f)\mathbf{f}, \tag{2.10}$$

where in two dimensions $\lambda_{(f)} = \lambda_{(2)}$, $\nabla = (\partial/\partial y_1)\hat{\mathbf{e}}_1 + (\partial/\partial y_2)\hat{\mathbf{e}}_2$, and $\hat{\mathbf{e}}_1$ and $\hat{\mathbf{e}}_2$ are unit normal vectors. If $\mathbf{f}$ is linear in $\mathbf{y}$, the eigenvectors in phase space are constant, and thus we have that $\nabla \tilde{\mathbf{V}}_f = \mathbf{0}$. Then from Eq. (2.10) it is evident that the normal to the ILDM is in the same direction as the vector $\tilde{\mathbf{V}}_f$, and hence, the vector $\mathbf{f}$ is tangent to the ILDM. To summarize for a linear system, the ILDM is a phase space trajectory as well as the SIM, and it is a linear subspace of the phase space defined by $\mathbf{z}_f = \tilde{\mathbf{V}}_f \mathbf{y} = 0$, as given by Eq. (2.7). For a nonlinear system the second term on the right hand side of Eq. (2.10) is nonzero and corresponds to a local measure of the curvature of the manifold; consequently, the normal to the ILDM is not in the same direction as the vector $\tilde{\mathbf{V}}_f$, nor is the vector $\mathbf{f}$ tangent to the ILDM. To summarize for a nonlinear system, the ILDM is not a trajectory in phase space, but, as long as a spectral gap exists, it can be deduced from Eq. (2.10) that in the limit of large $\|\mathbf{\Lambda}_{(f)}\|$, the deviation of the ILDM from the phase space trajectory and the SIM becomes small.

III. COMPARISON OF SIM WITH ILDM

If one assumes the existence of an m-dimensional SIM in an n-dimensional phase space, it can be described as

$$y_i = y_i(y_1, \ldots, y_m), \quad i = m+1, \ldots, n, \tag{3.1}$$

where $y_1, \ldots, y_m$ are the independent state variables chosen to parameterize the SIM, and $y_{m+1}, \ldots, y_n$ are the dependent state variables. The assumed form of the SIM is then differentiated to obtain

$$\frac{dy_i}{dt} = \sum_{j=1}^{m} \frac{\partial y_i}{\partial y_j} \frac{dy_j}{dt}, \quad i = m+1, \ldots, n. \tag{3.2}$$

All trajectories in phase space, including the m-dimensional SIM defined by Eq. (3.1), satisfy the following equation, which is obtained by eliminating time derivatives from Eq. (3.2) with the use of Eq. (2.1),

$$f_i(y_{m+1}, \ldots, y_n; y_1, \ldots, y_m) = \sum_{j=1}^{m} f_j(y_{m+1}, \ldots, y_n; y_1, \ldots, y_m) \times \frac{\partial y_i(y_1, y_2, \ldots, y_m)}{\partial y_j}, \quad i = m+1, \ldots, n. \tag{3.3}$$

Fraser[27] and Roussel and Fraser[28] have used functional iteration to solve Eq. (3.3). For each y_i, $i = m+1, \ldots, n$, an initial function of the form $y_i = y_i^0(y_1, \ldots, y_m)$ is chosen. Functional iteration is then performed on the following equations, which are obtained by rewriting Eq. (3.3),

$$\mathcal{G}_i\left(y_{m+1}^{k+1}, \ldots, y_n^{k+1}, \frac{\partial y_i^k}{\partial y_1}, \ldots, \frac{\partial y_i^k}{\partial y_m}; y_1, \ldots, y_m\right) = 0, \quad i = m+1, \ldots, n, \tag{3.4}$$

where the superscript indicates the iteration number starting from $k=0$. One can use computer algebra to perform functional iteration. For high dimensional systems and for systems where Eq. (3.4) is not explicit in y_i^{k+1}, $i = m+1, \ldots, n$, it is more convenient to use the modified method of Davis and Skodje,[29] which uses numerical functional iteration. A discrete form of initial functions $y_i^0(y_1, \ldots, y_m)$, $i = m+1, \ldots, n$, are now chosen in a domain $\mathcal{H}$ where the SIM is to be estimated, such that $(y_1, \ldots, y_m) \in \mathcal{H}$. For numerical computations, the domain $\mathcal{H}$ is discretized into a finite number of points, and partial derivatives in Eq. (3.4)

are approximated by finite differences. Numerical functional iteration is then performed on the resulting implicit algebraic equations. The choice of state variables used for parameterization of the SIM in Eq. (3.1) may be arbitrary, though it is essential that these variables be chosen in such a way that the manifold functions given in Eq. (3.1) are single-valued. A proper choice of parametric state variables makes numerical computations of the SIM easier. The functional iteration is expected to converge to the SIM if (a) the initial functional guess is good, (b) the initial guess does not correspond to a phase space trajectory, and (c) there exists an attractive SIM in the phase space as assumed. Both Davis and Skodje,[29] and Roussel,[39] and Roussel and Fraser[40] have suggested methods to enhance the stability of the numerical and algebraic functional iterations, respectively.

Davis and Skodje,[29] using a simple example, have illustrated the difference between the ILDM and the SIM. Their two-dimensional system, of the form of Eq. (2.1), is analogous to a system which models a spatially premixed homogeneous reactor and is given by

$$\frac{d}{dt}\begin{pmatrix} y_1 \\ y_2 \end{pmatrix} = \begin{pmatrix} -y_1 \\ -\gamma y_2 + \dfrac{(\gamma-1)y_1 + \gamma y_1^2}{(1+y_1)^2} \end{pmatrix}, \tag{3.5}$$

where $\gamma > 1$ gives a measure of stiffness for the system. If γ is increased, stiffness will increase. The Jacobian of the right-hand side is

$$\mathbf{J} = \begin{pmatrix} -1 & 0 \\ \dfrac{\gamma-1+(\gamma+1)y_1}{(1+y_1)^3} & -\gamma \end{pmatrix}, \tag{3.6}$$

and has eigenvalues $(\lambda_{(1)}, \lambda_{(2)}) = (-1, -\gamma)$. The right eigenvectors and their reciprocal vectors are given by

$$\mathbf{V} = (\mathbf{V}_s \vdots \mathbf{V}_f) = \begin{pmatrix} 1 & \vdots & 0 \\ \dfrac{\gamma-1+(\gamma+1)y_1}{(\gamma-1)(1+y_1)^3} & \vdots & 1 \end{pmatrix}, \tag{3.7}$$

$$\tilde{\mathbf{V}} = \begin{pmatrix} \tilde{\mathbf{V}}_s \\ \vdots \\ \tilde{\mathbf{V}}_f \end{pmatrix} = \begin{pmatrix} 1 & 0 \\ \cdots & \cdots \\ -\dfrac{\gamma-1+(\gamma+1)y_1}{(\gamma-1)(1+y_1)^3} & 1 \end{pmatrix}.$$

Equation (2.8) is used to determine the one-dimensional ILDM for this system, which can be written in closed form,

$$y_2 = \frac{y_1}{1+y_1} + \frac{2y_1^2}{\gamma(\gamma-1)(1+y_1)^3}. \tag{3.8}$$

The slow, $\tilde{\mathbf{V}}_s(d\mathbf{y}/dt) = \tilde{\mathbf{V}}_s\mathbf{f}$, and fast, $\tilde{\mathbf{V}}_f(d\mathbf{y}/dt) = \tilde{\mathbf{V}}_f\mathbf{f}$, equations for this example are given, respectively, by

$$\frac{dy_1}{dt} = -y_1, \tag{3.9a}$$

$$\frac{1}{\gamma}\left(-\frac{\gamma-1+(\gamma+1)y_1}{(\gamma-1)(1+y_1)^3}\frac{dy_1}{dt} + \frac{dy_2}{dt} \right) = -y_2 + \frac{y_1}{1+y_1} + \frac{2y_1^2}{\gamma(\gamma-1)(1+y_1)^3}. \tag{3.9b}$$

The order of the terms on both sides of Eq. (3.9b) can be represented by

$$\mathcal{O}(\gamma^{-1}) + \mathcal{O}(\gamma^{-2}) + \cdots = \mathcal{O}(1) + \mathcal{O}(\gamma^{-1}) + \mathcal{O}(\gamma^{-2}) + \cdots. \tag{3.10}$$

The standard ILDM approximation neglects all terms on the left-hand side of the fast equation while retaining all terms on the right-hand side. This makes the ILDM an inconsistent approximation to the SIM. On the other hand a systematic matching of terms of all orders will correctly lead to the SIM. This is demonstrated by Kaper and Kaper.[26] However, it is not clear how to implement a systematic perturbation analysis for a system where parameters such as γ^{-1} are difficult to define explicitly and globally in composition space. This is the case in complicated systems of chemical kinetics, where γ plays the role of the magnitude of fast eigenvalues. In such systems, the order of eigenvalues and their membership in the slow and fast sets change with time!

Here we solve Eq. (3.3) using an approach often used in center manifold theory.[37] The SIM is assumed to exist and have the following polynomial form:

$$y_2 = y_2(y_1) = \sum_{k=0}^{\infty} c_k y_1^k, \tag{3.11}$$

where c_k are constant coefficients. Equation (3.3), in this case, is given by

$$-\gamma y_2 + \frac{(\gamma-1)y_1 + \gamma y_1^2}{(1+y_1)^2} = \frac{dy_2}{dy_1}(-y_1). \tag{3.12}$$

Substituting Eq. (3.11) in Eq. (3.12), we obtain the following coefficients for the SIM:

$$c_0 = 0, \quad c_k = (-1)^{k+1}, \quad k = 1, \ldots, \infty. \tag{3.13}$$

Hence, the SIM is given by

$$y_2 = y_1(1 - y_1 + y_1^2 - y_1^3 + y_1^4 + \cdots) = \frac{y_1}{1+y_1}. \tag{3.14}$$

When the ILDM in Eq. (3.8) is compared with the SIM in Eq. (3.14) for this simple system, it is obvious that (1) the ILDM is *not* a SIM, and (2) the error in the ILDM approximation decreases as γ increases. Though the assumption for the SIM to be of polynomial form, as in Eq. (3.11), works well in this example, it may not work for more complicated systems. This is primarily because such a representation of the SIM is only accurate sufficiently close to the equilibrium point and, in general, diverges rapidly away from it. To find the global SIM for more complicated systems, we have to resort to numerical computations such as those proposed by Davis and Skodje.[29]

The inconsistency in the ILDM procedure in matching of terms of similar orders, leads to errors as shown in this

simple system. We emphasize that the error in the ILDM approximation is small only for systems in which the spectral gap condition $|\lambda_{(m)}|/|\lambda_{(m+1)}| \ll 1$ is valid. Fortunately this situation arises frequently in complicated systems associated with chemical kinetics. Also, in our experience, the numerical computation of the ILDM is more tractable in its implementation than the numerical computation of the SIM.

IV. REACTIVE FLOW EQUATIONS

The governing equations for a one-dimensional reacting flow system can be written in the following compact form,

$$\frac{\partial \mathbf{y}}{\partial t} = \mathbf{f}(\mathbf{y}) - \frac{\partial}{\partial x}(\mathbf{h}(\mathbf{y})), \tag{4.1}$$

where $\mathbf{y} \in \mathcal{R}^n$ represents a set of dependent variables, $\mathbf{h}(\mathbf{y})$ represents the convective and diffusive flux vector, and $\mathbf{f}(\mathbf{y})$ represents the reaction source term. The independent time and space variables are t and x, respectively.

We again rewrite the reaction-diffusion equations in terms of a new set of variables defined by $\mathbf{z} = \tilde{\mathbf{V}}\mathbf{y}$. The eigenvector matrix of the Jacobian of the source term $\mathbf{f}$ is represented by $\mathbf{V}$ and is again defined by Eq. (2.2). We note that this basis, $\mathbf{V}$, is derived solely from the chemistry of a spatially homogeneous system. While this will eventually lead to an improved estimation of the system's behavior, a better basis on which to project would take account of the infinite-dimensional eigenfunctions associated with the convection-diffusion operator. This, however, is difficult.

We can then rewrite Eq. (4.1) as

$$\frac{1}{\lambda_{(i)}}\left(\frac{dz_i}{dt} + \tilde{\mathbf{v}}_i \sum_{j=1}^{n} \frac{d\mathbf{v}_j}{dt} z_j\right) = z_i + \frac{1}{\lambda_{(i)}}(\tilde{\mathbf{v}}_i \mathbf{g}) - \frac{1}{\lambda_{(i)}}\left(\tilde{\mathbf{v}}_i \frac{\partial \mathbf{h}}{\partial x}\right), \quad i = 1, \ldots, n. \tag{4.2}$$

We again assume that we are only interested in the dynamics of the processes occurring at time scales of $1/|\lambda_{(m)}|$ or slower and that a spectral gap exists. Hence, we assume that all other processes occurring at faster time scales can be neglected and are equilibrated by neglecting the left hand side, which is $\mathcal{O}(1/|\lambda_{(m+1)}|)$ or smaller, of Eq. (4.2) for $i = m+1, \ldots, n$, while the right-hand side is $\mathcal{O}(1)$ or larger for the same. Hence, the following is obtained:

$$z_i + \frac{1}{\lambda_{(i)}}(\tilde{\mathbf{v}}_i \mathbf{g}) - \frac{1}{\lambda_{(i)}}\left(\tilde{\mathbf{v}}_i \frac{\partial \mathbf{h}}{\partial x}\right) = 0, \quad i = m+1, \ldots, n. \tag{4.3}$$

If convection and diffusion processes occur at time scales which are slower than reaction time scales of order $1/|\lambda_{(m+1)}|$, then we can neglect the third term $1/\lambda_{(i)}(\tilde{\mathbf{v}}_i(\partial \mathbf{h}/\partial x))$ in Eq. (4.3), as it becomes $\mathcal{O}(1/|\lambda_{(m+1)}|)$ or smaller while the remaining terms are $\mathcal{O}(1)$ or larger, and obtain Eq. (2.7). Instead, if convection and diffusion time scales overlap with fast chemical time scales, then we cannot make such an approximation as the third term in Eq. (4.3) will become $\mathcal{O}(1)$ or larger. No robust analysis exists to determine convection and diffusion time scales *a priori*. We assume that convection and diffusion processes occur at time scales of $1/|\lambda_{(p)}|$ for $m < p < n$ and slower. Then by equilibrating the fast dynamics, we obtain the differential algebraic system of equations given by

$$z_i + \frac{1}{\lambda_{(i)}}(\tilde{\mathbf{v}}_i \mathbf{g}) - \frac{1}{\lambda_{(i)}}\left(\tilde{\mathbf{v}}_i \frac{\partial \mathbf{h}}{\partial x}\right) = 0, \quad i = m+1, \ldots, p, \tag{4.4a}$$

$$z_i + \frac{1}{\lambda_{(i)}}(\tilde{\mathbf{v}}_i \mathbf{g}) = 0, \quad i = p+1, \ldots, n. \tag{4.4b}$$

These equations can be rewritten in a more convenient form as

$$\tilde{\mathbf{V}}_{fs}\mathbf{f} - \tilde{\mathbf{V}}_{fs}\frac{\partial \mathbf{h}}{\partial x} = \mathbf{0}, \tag{4.5a}$$

$$\tilde{\mathbf{V}}_{ff}\mathbf{f} = \mathbf{0}, \tag{4.5b}$$

where now

$$\tilde{\mathbf{V}}_f = \begin{pmatrix} - & \tilde{\mathbf{v}}_{m+1} & - \\ & \vdots & \\ - & \tilde{\mathbf{v}}_p & - \\ \cdots & \cdots & \cdots \\ - & \tilde{\mathbf{v}}_{p+1} & - \\ & \vdots & \\ - & \tilde{\mathbf{v}}_n & - \end{pmatrix} = \begin{pmatrix} \tilde{\mathbf{V}}_{fs} \\ \cdots \\ \tilde{\mathbf{V}}_{ff} \end{pmatrix}, \tag{4.6}$$

where the matrix $\tilde{\mathbf{V}}_{fs}$ has dimension $(p-m) \times n$ and its row vectors contain the reciprocal vectors of the right eigenvectors associated with the time scales $1/|\lambda_{(m+1)}|, \ldots, 1/|\lambda_{(p)}|$, and the matrix $\tilde{\mathbf{V}}_{ff}$ has dimension $(n-p) \times n$ and its row vectors contain the reciprocal vectors of the right eigenvectors associated with the time scales $1/|\lambda_{(p+1)}|, \ldots, 1/|\lambda_{(n)}|$. Equations (4.5) represent the *infinite-dimensional* Approximate Slow Invariant Manifold (ASIM) on which the slow dynamics occurs once all fast time scale processes have equilibrated. Equations (4.5) correspond to a system of differential algebraic equations which have to be solved in physical space dimensions together with the prescribed boundary conditions. Hence, the slow dynamics for Eq. (4.1) is approximated by integrating the following set of partial differential algebraic equations:

$$\tilde{\mathbf{V}}_s \frac{\partial \mathbf{y}}{\partial t} = \tilde{\mathbf{V}}_s \mathbf{f} - \tilde{\mathbf{V}}_s \frac{\partial \mathbf{h}}{\partial x}, \tag{4.7a}$$

$$\mathbf{0} = \tilde{\mathbf{V}}_{fs}\mathbf{f} - \tilde{\mathbf{V}}_{fs}\frac{\partial \mathbf{h}}{\partial x}, \tag{4.7b}$$

$$\mathbf{0} = \tilde{\mathbf{V}}_{ff}\mathbf{f}. \tag{4.7c}$$

The reduced PDEs in Eq. (4.7a) describe the time evolution of the slow dynamics, and are solved in conjunction with Eqs. (4.7b) and (4.7c) describing the ASIM. The ASIM is an infinite dimensional manifold which accounts for the effects of convection and diffusion. The stiffness due to the reaction source term in Eq. (4.1) is substantially reduced in Eqs. (4.7).

It is obvious that for two- and three-dimensional reactive flow equations the ASIM is described by a set of elliptic partial differential algebraic equations.

V. A SIMPLE EXAMPLE

We extend the simple system in Eq. (3.5) by including diffusion effects in one spatial dimension so as to obtain an equation of the form of Eq. (4.1). Specifically we take $\mathbf{y}$, $\mathbf{f}(\mathbf{y})$, and $\mathbf{h}(\mathbf{y})$ so as to obtain the following system of equations:

$$\frac{\partial y_1}{\partial t} = -y_1 + \mathcal{D}\frac{\partial^2 y_1}{\partial x^2}, \tag{5.1a}$$

$$\frac{\partial y_2}{\partial t} = -\gamma y_2 + \frac{(\gamma-1)y_1 + \gamma y_1^2}{(1+y_1)^2} + \mathcal{D}\frac{\partial^2 y_2}{\partial x^2}. \tag{5.1b}$$

The chemical time scales are 1 and γ^{-1}, while the diffusion time scale depends on the parameter $\mathcal{D}$ and local spatial gradients. The ILDM for this system is given by Eq. (3.8). We choose a spatial domain $x \in [0,1]$ and the following boundary conditions which lie on the ILDM:

$$\mathbf{y}(t,0) = \begin{pmatrix} 0 \\ 0 \end{pmatrix}, \quad \mathbf{y}(t,1) = \begin{pmatrix} 1 \\ \frac{1}{2} + \frac{1}{4\gamma(\gamma-1)} \end{pmatrix}. \tag{5.2}$$

The reason for choosing the boundary conditions to lie on the ILDM will be clarified later. The following initial conditions are chosen which, for convenience only, linearly interpolate between the two boundary conditions,

$$\mathbf{y}(0,x) = \begin{pmatrix} x \\ \left(\frac{1}{2} + \frac{1}{4\gamma(\gamma-1)}\right)x \end{pmatrix}. \tag{5.3}$$

Figure 2 depicts results at time $t=5$ for the integration of the full system of Eqs. (5.1), for $\mathcal{D}=0.1$, 0.01 and $\gamma=10$. The numerical computations are done using a uniform grid of 100 points in the spatial dimension x. A central difference approximation of second order is used for spatial discretization. A backward difference formula (BDF) of second order accuracy in time is used for time advancement with the aid of the LSODE (Ref. 41) package. The solution is plotted in the two-dimensional phase space of the dependent variables. Stars represent the solution at various grid points in physical space. The time $t=5$ is long enough for the fast time scales to equilibrate; in fact, the system is close to steady state. It can be seen from the figures that the steady state solution does not lie on the the ILDM. Hence, forcing the solution onto the ILDM, or approximating the slow dynamics of Eqs. (5.1) by the ILDM, will lead to large errors. The effect of reducing the value of $\mathcal{D}$ is the appearance of sharper gradients in the solution in physical space. The maximum, or the $\mathbf{L}_\infty$ norm, of the difference between the full solution and the ILDM for fixed γ is seen in Fig. 3 to remain large even when $\mathcal{D}$ is decreased.

Figure 4 depicts results at time $t=5$, for the integration of the full system of Eqs. (5.1), for $\gamma=100$ and $\mathcal{D}=0.1$. It can be seen that for this case the solution is closer to the

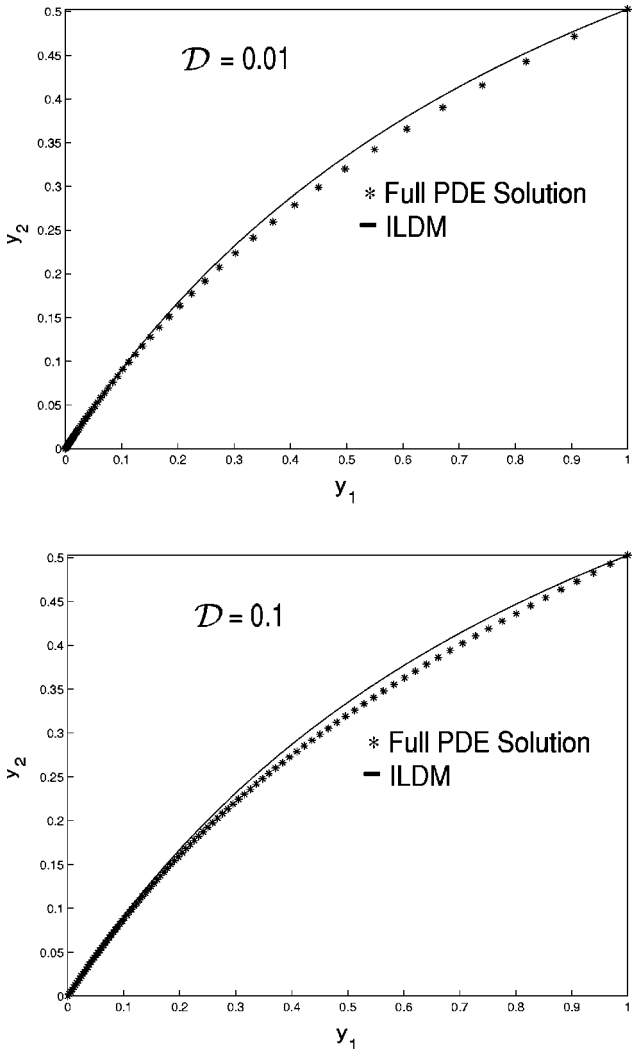

FIG. 2. Comparison of solution of the full PDEs at $t=5$ with the ILDM, for $\gamma=10$ and $\mathcal{D}=0.01$, 0.1, for Davis and Skodje's (Ref. 29) model problem extended to include diffusion.

ILDM primarily because the diffusion term in Eq. (4.3) has a smaller effect. Hence, the slow dynamics are better approximated by the ILDM for large γ. The $\mathbf{L}_\infty$ norm of the difference between the full solution and the ILDM for fixed $\mathcal{D}$ is seen in Fig. 5 to decrease as γ, or the stiffness due to the reaction source term $\mathbf{f}(\mathbf{y})$, increases.

The slow dynamics for Eqs. (5.1), obtained by using the ASIM as done in Eqs. (4.7), for $n=2$, $m=1$ and $p=n$, is given by

$$\frac{\partial y_1}{\partial t} = -y_1 + \mathcal{D}\frac{\partial^2 y_1}{\partial x^2}, \tag{5.4a}$$

$$0 = -y_2 + \frac{y_1}{1+y_1} + \frac{2y_1^2}{\gamma(\gamma-1)(1+y_1)^3} - \left(\frac{\gamma-1+(\gamma+1)y_1}{\gamma(\gamma-1)(1+y_1)^3}\right)\mathcal{D}\frac{\partial^2 y_1}{\partial x^2} + \frac{1}{\gamma}\mathcal{D}\frac{\partial^2 y_2}{\partial x^2}. \tag{5.4b}$$

We will compare the solution obtained by Eqs. (5.4) to the solution obtained by integration of the full system of Eqs.

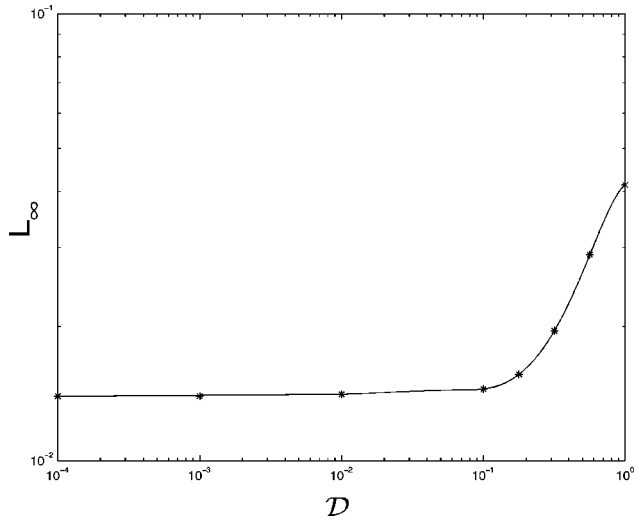

FIG. 3. Maximum error ($\mathbf{L}_\infty[0,1]$) between solution of the full PDEs at $t=5$ and the ILDM, for fixed $\gamma=10$ and varying $\mathcal{D}$, for Davis and Skodje's (Ref. 29) model problem extended to include diffusion. Stars indicate the values of $\mathcal{D}$ for which the computations were done.

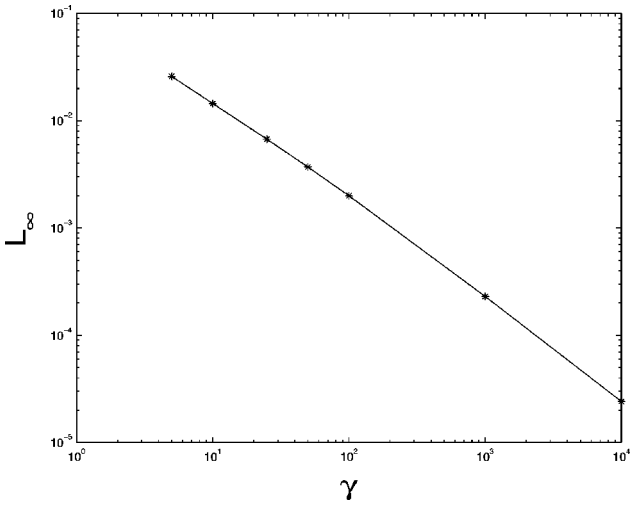

FIG. 5. Maximum error ($\mathbf{L}_\infty[0,1]$) between solution of the full PDEs at $t=5$ and the ILDM, for varying γ and fixed $\mathcal{D}=0.1$, for Davis and Skodje's (Ref. 29) model problem extended to include diffusion. Stars indicate the values of γ for which the computations were done.

(5.1). Note that the boundary conditions and initial condition for $y_1(t,x)$ are the same as before, but the initial condition $y_2(0,x)$ must be chosen such that Eq. (5.4b), which represents the ASIM for the system, is satisfied for given $y_1(0,x)$. That is, the initial condition is chosen so that it lies on the ASIM and minimizes the phase error that might occur if an arbitrary initial condition is used. Equation (5.4b) with boundary conditions given in Eq. (5.2) constitute a two-point boundary value problem which can be written in the form,

$$\mathbf{L}y_2=F(y_1(t,x)), \quad y_2(t,0)=0,$$
$$y_2(t,1)=\frac{1}{2}+\frac{1}{4\gamma(\gamma-1)}, \tag{5.5}$$

where

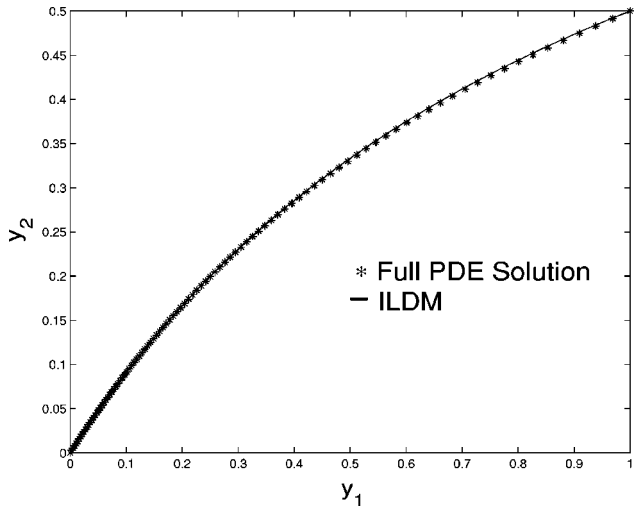

FIG. 4. Comparison of solution of the full PDEs at $t=5$ with the ILDM, for $\gamma=100$ and $\mathcal{D}=0.1$, for Davis and Skodje's (Ref. 29) model problem extended to include diffusion.

$$\mathbf{L}=\frac{\partial^2}{\partial x^2}-\frac{\gamma}{\mathcal{D}}, \tag{5.6}$$

$$F(y_1(t,x))=-\frac{\gamma}{\mathcal{D}}\left(\frac{y_1}{1+y_1}+\frac{2y_1^2}{\gamma(\gamma-1)(1+y_1)^3}-\left(\frac{\gamma-1+(\gamma+1)y_1}{\gamma(\gamma-1)(1+y_1)^3}\mathcal{D}\frac{\partial^2 y_1}{\partial x^2}\right)\right), \tag{5.7}$$

the solution of which is given by

$$y_2(t,x)=\left(\frac{1}{2}+\frac{1}{4\gamma(\gamma-1)}\right)\frac{\sinh\left(\sqrt{\frac{\gamma}{\mathcal{D}}}\,x\right)}{\sinh\left(\sqrt{\frac{\gamma}{\mathcal{D}}}\right)}+\int_0^1 G(x,s)F(y_1(t,s))ds, \tag{5.8}$$

where the Green's function $G(x,s)$ is given by

$$G(x,s)=\begin{cases}\dfrac{\sinh\left(\sqrt{\frac{\gamma}{\mathcal{D}}}(s-1)\right)\sinh\left(\sqrt{\frac{\gamma}{\mathcal{D}}}x\right)}{\sqrt{\frac{\gamma}{\mathcal{D}}}\sinh\left(\sqrt{\frac{\gamma}{\mathcal{D}}}\right)}, & 0\leqslant x\leqslant s,\\ \dfrac{\sinh\left(\sqrt{\frac{\gamma}{\mathcal{D}}}(x-1)\right)\sinh\left(\sqrt{\frac{\gamma}{\mathcal{D}}}s\right)}{\sqrt{\frac{\gamma}{\mathcal{D}}}\sinh\left(\sqrt{\frac{\gamma}{\mathcal{D}}}\right)}, & s\leqslant x\leqslant 1.\end{cases} \tag{5.9}$$

Maas and Pope[32] have proposed a different projection (MPP) method when the diffusion time scales are of the order of the slow chemical time scales and much slower than the fast chemical time scales. They assume that diffusion

processes perturb the system off the ILDM, but it rapidly relaxes back to the ILDM due to the fast chemistry. This procedure is implemented by the following projection of the convection diffusion term in Eq. (4.1) along the local slow subspace on the reaction ILDM,

$$\frac{\partial \mathbf{y}}{\partial t} = \mathbf{f}(\mathbf{y}) - \mathbf{V}_s \tilde{\mathbf{V}}_s \frac{\partial}{\partial x}(\mathbf{h}(\mathbf{y})). \tag{5.10}$$

The corresponding equations for the example are then given by

$$\frac{\partial y_1}{\partial t} = -y_1 + \mathcal{D}\frac{\partial^2 y_1}{\partial x^2}, \tag{5.11a}$$

$$\frac{\partial y_2}{\partial t} = -\gamma y_2 + \frac{(\gamma-1)y_1 + \gamma y_1^2}{(1+y_1)^2} - \left(\frac{\gamma - 1 + (\gamma+1)y_1}{\gamma(\gamma-1)(1+y_1)^3}\right)\mathcal{D}\frac{\partial^2 y_1}{\partial x^2}. \tag{5.11b}$$

One then solves either of the Eqs. (5.11a) or (5.11b) along with the ILDM Eq. (3.8). Hence, the slow dynamics for the MPP method is described by

$$\frac{\partial y_1}{\partial t} = -y_1 + \mathcal{D}\frac{\partial^2 y_1}{\partial x^2}, \tag{5.12a}$$

$$y_2 = \frac{y_1}{1+y_1} + \frac{2y_1^2}{\gamma(\gamma-1)(1+y_1)^3}. \tag{5.12b}$$

We see that the MPP method effectively chooses $n=2$ and $m=p=1$. Hence, the MPP method forces the solution onto the finite dimensional ILDM, which will incur a large error for the cases depicted in Fig. 2. Equation (5.12b) of the MPP method has as its analog Eq. (5.8) of the ASIM method. It is clear that Eq. (5.8) accounts for slow reaction, diffusion, and boundary conditions, while Eq. (5.12b) only accounts for slow reaction.

Figure 6 compares the solution obtained by full integration, use of the ASIM and the MPP method, all using a fixed grid of 100 points, with the baseline solution obtained by full integration at high spatial resolution of 10 000 points. The computations are for $\gamma=10$ and $\mathcal{D}=0.1$. The numerical scheme used is the same as described previously. Use of an implicit time stepping scheme is not required when using the ASIM or the MPP method. Also, larger time increments can be used for the solution of Eqs. (5.4a) and (5.8) when using the ASIM and Eqs. (5.12) for the MPP method, than that for the solution of Eqs. (5.1), if explicit numerical methods are used, due to the reduced stiffness in the equations. However, since the accuracy of the three methods is to be compared, the numerical solutions of all the three methods are obtained using the same LSODE package with the same time increments until steady state is achieved. Note that a numerical quadrature of Eq. (5.8) is done in the ASIM procedure. The $\mathbf{L}_2$ norm of the errors between the solutions obtained by the three methods and the baseline solution at various times have been plotted. When full integration is used, discretization error is incurred as the 100 grid points used for the computation are substantially fewer than those used for the computation of the baseline solution. At steady state, the error in the full integration method becomes constant. The initial error incurred when using the ASIM is due to the fact that the solution from the initial condition takes some time to relax to the ASIM. Near steady state the error incurred when using the ASIM and the error incurred by full integration are essentially identical. A large error is incurred by the MPP method in both transient and steady state periods. This is due to the fact that this method forces the solution onto the finite dimensional ILDM even though the solution does not lie on it. It can be seen that the overall error incurred when using the ASIM is substantially less than the error incurred when using the MPP method.

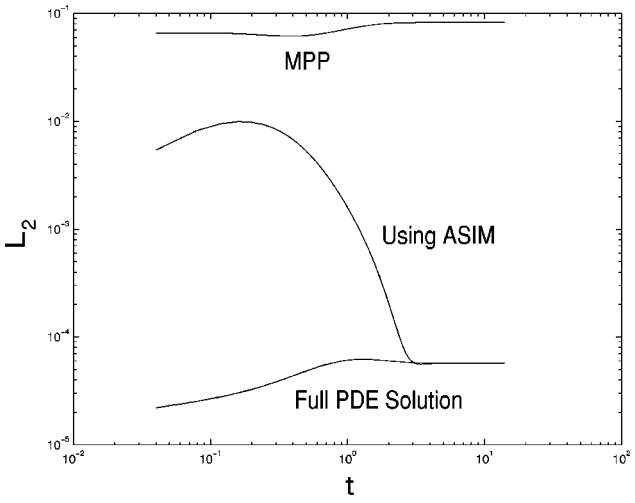

FIG. 6. Comparison of errors incurred by the three methods at a resolution of 100 grid points relative to a baseline solution of full integration at a resolution of 10 000 grid points, for $\gamma=10$ and $\mathcal{D}=0.1$, for Davis and Skodje's (Ref. 29) model problem extended to include diffusion.

If the boundary conditions were not chosen on the ILDM, then the MPP method would incur larger errors, as that would further cause the solution to not lie on the ILDM. On the other hand, errors incurred when using the ASIM will not be affected by the choice of the boundary conditions. Figure 7 depicts the solutions in the phase space at time $t=5$, obtained using the three methods, for a case where one of the boundary condition, $y_2(t,1)=\frac{3}{4}$, does not lie on the ILDM. It can be seen that the error in the solution obtained by the MPP method will always remain large near the boundary at $x=1$ which does not lie on the ILDM. In the earlier case for which the errors are plotted in Fig. 6, the error due to the boundary conditions in the MPP method is eliminated so as to separate these errors.

VI. PREMIXED LAMINAR FLAME FOR OZONE DECOMPOSITION

The governing equations which model the time-dependent, one-dimensional, isobaric, premixed laminar flame for ozone decomposition in Lagrangian coordinates are derived from the Navier–Stokes equations under the assumptions of low Mach number,[42]

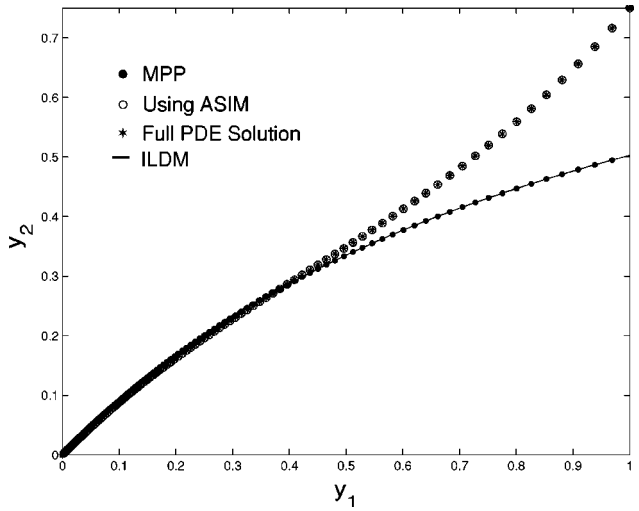

FIG. 7. Comparison of solutions obtained by full integration, using the ASIM and the MPP method at $t=5$, for $\gamma=10$ and $\mathcal{D}=0.1$, for a case where the boundary condition at $x=1$ does not lie on the ILDM.

$$\frac{\partial T}{\partial t}+\dot{m}_0\frac{\partial T}{\partial \psi}=-\frac{1}{\rho c_p}\sum_{k=1}^{3}\dot{\omega}_k M_k h_k+\frac{1}{c_p}\frac{\partial}{\partial \psi}\left(\rho\lambda\frac{\partial T}{\partial \psi}\right)+\sum_{k=1}^{3}\frac{c_p^k}{c_p}\rho^2\mathcal{D}_k\frac{\partial Y_k}{\partial \psi}\frac{\partial T}{\partial \psi}, \tag{6.1a}$$

$$\frac{\partial Y_k}{\partial t}+\dot{m}_0\frac{\partial Y_k}{\partial \psi}=\frac{1}{\rho}\dot{\omega}_k M_k+\frac{\partial}{\partial \psi}\left(\rho^2\mathcal{D}_k\frac{\partial Y_k}{\partial \psi}\right),\quad k=1,2,3, \tag{6.1b}$$

where the dependent variables are the fluid temperature T and the mass fractions in the fluid mixture, Y_1, Y_2, and Y_3, of oxygen atom O, oxygen molecule O_2, and ozone molecule O_3, respectively. The terms M_k and c_p^k represent the molecular mass and the specific heat capacity at constant pressure, respectively, of species k. The mass averaged specific heat capacity at constant pressure of the fluid mixture is given by $c_p=\Sigma_{k=1}^{3}Y_k c_p^k$. The specific enthalpy of species k is given by $h_k=h_{0k}+\int_{T_0}^{T}c_p^k dT$, where h_{0k} is the standard enthalpy of formation per unit mass of species k at the standard temperature $T_0=298$ K. The diffusion coefficient of species k into the fluid mixture is $\mathcal{D}_k$, while the thermal conductivity of the fluid mixture is λ. The mixture density is ρ. The independent variables are time t, and the Lagrangian coordinate ψ, where

$$\psi(t,x)=\int_0^x \rho(t,\tilde{x})d\tilde{x}, \tag{6.2}$$

where x is the spatial coordinate. The inlet mass flow rate, $\dot{m}_0$, is given by

$$\dot{m}_0(t)=\rho u|_{x=0}, \tag{6.3}$$

where u is the flow velocity. The molar rate of production of species k per unit volume, $\dot{\omega}_k$, is given by the law of mass action with Arrhenius kinetics,

TABLE I. Three-species, 14-step reaction mechanism for ozone decomposition (Ref. 42) Units of a_j are in appropriate combinations of cm, mol, s, and K so that $\dot{\omega}_k$ has units of mol cm^{-3} s^{-1}; units of E_j are in erg mol^{-1}.

j	Reaction	a_j	β_j	E_j
1	$O_3+O\rightarrow O_2+O+O$	6.76×10^6	2.50	1.01×10^{12}
2	$O_2+O+O\rightarrow O_3+O$	1.18×10^2	3.50	0.00
3	$O_3+O_2\rightarrow O_2+O+O_2$	6.76×10^6	2.50	1.01×10^{12}
4	$O_2+O+O_2\rightarrow O_3+O_2$	1.18×10^2	3.50	0.00
5	$O_3+O_3\rightarrow O_2+O+O_3$	6.76×10^6	2.50	1.01×10^{12}
6	$O_2+O+O3\rightarrow O_3+O_3$	1.18×10^2	3.50	0.00
7	$O+O_3\rightarrow 2O_2$	4.58×10^6	2.50	2.51×10^{11}
8	$2O_2\rightarrow O+O_3$	1.88×10^6	2.50	4.15×10^{12}
9	$O_2+O\rightarrow 2O+O$	5.71×10^6	2.50	4.91×10^{12}
10	$2O+O\rightarrow O_2+O$	2.47×10^2	3.50	0.00
11	$O_2+O_2\rightarrow 2O+O_2$	5.71×10^6	2.50	4.91×10^{12}
12	$2O+O_2\rightarrow O_2+O_2$	2.47×10^2	3.50	0.00
13	$O_2+O_3\rightarrow 2O+O_3$	5.71×10^6	2.50	4.91×10^{12}
14	$2O+O_3\rightarrow O_2+O_3$	2.47×10^2	3.50	0.00

$$\dot{\omega}_k=\sum_{j=1}^{J}a_j T^{\beta_j}\exp\left(\frac{-E_j}{\Re T}\right)(\nu''_{kj}-\nu'_{kj})\prod_{i=1}^{N}\left(\frac{\rho Y_i}{M_i}\right)^{\nu'_{ij}},\quad k=1,\ldots,N, \tag{6.4}$$

where $J=14$ is the number of elementary reaction steps in the ozone decomposition reaction mechanism and $N=3$ is the number of species. The constant parameters a_j, β_j, E_j, ν'_{kj}, ν''_{kj}, and $\Re$ represent the kinetics rate constant of reaction j, the temperature dependence exponent of reaction j, the activation energy of reaction j, the stoichiometric coefficient of the kth species in reaction j of the reactants and products, and the universal gas constant ($\Re=8.314\,41\times10^7$ erg mol^{-1} K^{-1}), respectively. The elementary reaction steps in the ozone decomposition reaction mechanism, with the associated parameters, are given in Table I. The system of Eqs. (6.1) are closed using the ideal gas equation of state

$$p_0=\rho\Re T\sum_{k=1}^{3}\frac{Y_k}{M_k}, \tag{6.5}$$

where $p_0=8.32\times10^5$dyn/cm^2 is the constant pressure.

Following Margolis,[42] the governing equations are simplified using the following assumptions and constants:

$$\mathcal{D}_1=\mathcal{D}_2=\mathcal{D}_3=\mathcal{D}, \tag{6.6a}$$

$$\rho^2\mathcal{D}=4.336\times10^{-7}\ \text{g}^2/(\text{cm}^4\,\text{s}), \tag{6.6b}$$

$$\rho\lambda=4.579\times10^{-2}\ \text{g}^2/(\text{cm}^2\,\text{s}^3\,\text{K}), \tag{6.6c}$$

$$c_p^1=c_p^2=c_p^3=c_p=1.056\times10^7\ \text{erg}/(\text{g K}), \tag{6.6d}$$

$$M_1=16\ \text{g/mol},\quad M_2=32\ \text{g/mol},\quad M_1=48\ \text{g/mol}, \tag{6.6e}$$

$$h_{01}=1.534\times10^{11}\ \text{erg/g},\quad h_{02}=0\ \text{erg/g},\quad h_{03}=3.011\times10^{10}\ \text{erg/g}. \tag{6.6f}$$

The initial and the boundary conditions are applied in a frame of reference in which the fluid is initially at rest. A semi-infinite computational domain is considered with the following boundary conditions:

$$\frac{\partial T}{\partial \psi}=\frac{\partial Y_1}{\partial \psi}=\frac{\partial Y_2}{\partial \psi}=\frac{\partial Y_3}{\partial \psi}=0, \quad \text{for} \quad \psi=0,\infty \quad \text{and} \quad t\geqslant 0. \tag{6.7}$$

These conditions are equivalent to zero flux of thermal energy and species mass at $\psi=0,\infty$, which also leads to $u(t,0)=0$, and hence, $\dot{m}_0=0$. Using these assumptions with a unity Lewis number and nondimensionalization as done in Margolis,[42] Eqs. (6.1) can be simplified to

$$\frac{\partial T^*}{\partial t^*}=-\frac{1}{\rho^*}\sum_{k=1}^{3}\dot{\omega}_k^* M_k^* h_k^*+\frac{\partial^2 T^*}{\partial \psi^{*2}}, \tag{6.8a}$$

$$\frac{\partial Y_k}{\partial t^*}=\frac{1}{\rho^*}\dot{\omega}_k^* M_k^*+\frac{\partial^2 Y_k}{\partial \psi^{*2}}, \quad k=1,2,3, \tag{6.8b}$$

where the star superscript denotes nondimensional quantities.

The governing equations can be further simplified by replacing the species evolution equation for $k=2$, in Eq. (6.8b), by the following algebraic equation for the mass fractions:

$$\sum_{k=1}^{3} Y_k=1. \tag{6.9}$$

The total enthalpy h^* of the fluid mixture, in its nondimensional form, is given by the following equation:

$$h^*=\sum_{k=1}^{3} Y_k h_k^*=\sum_{k=1}^{3} Y_k h_{0k}^*+T^*-T_0^*. \tag{6.10}$$

Using Eqs. (6.9)–(6.10) with Eqs. (6.8) and boundary conditions in Eq. (6.7) we obtain

$$\frac{\partial h^*}{\partial t^*}=\frac{\partial^2 h^*}{\partial \psi^{*2}}, \quad \text{with} \quad \frac{\partial h^*}{\partial \psi^*}(t^*,0)=\frac{\partial h^*}{\partial \psi^*}(t^*,\infty)=0. \tag{6.11}$$

If the initial conditions are chosen such that $h^*(0,\psi^*)=h_r^*$, where h_r^* is the total specific enthalpy of the reactant mixture, then Eq. (6.11) ensures that there is no tendency for the total specific enthalpy of the fluid mixture to change from its uniform initial value, and thus remains constant for all ψ^* and t^*. Hence, Eq. (6.8a) can be replaced by the following Schwab–Zeldovich relation:

$$T^*=T_0^*+h_r^*-\sum_{k=1}^{3} Y_k h_{0k}^*. \tag{6.12}$$

Therefore, we require the solution of only two PDEs from Eq. (6.8b), for $k=1$ and 3 (O and O_3), coupled with algebraic Eqs. (6.9) and (6.12).

A computational domain of finite length is chosen from $\psi^*=0$ to 2000. The following initial and boundary conditions are chosen:

$$Y_1(0,\psi^*)=0, \quad 0\leqslant \psi^*\leqslant 2000, \tag{6.13a}$$

$$Y_3(0,\psi^*)=0.15, \quad 0\leqslant \psi^*\leqslant 300, \tag{6.13b}$$

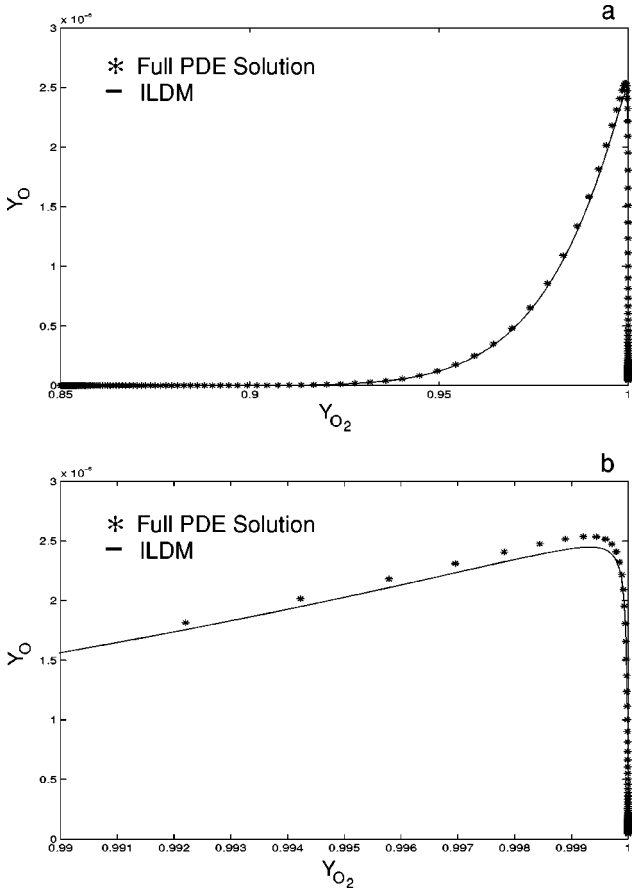

FIG. 8. Comparison of the steady state solution of the full PDEs with the ILDM in the phase space for ozone decomposition laminar flame: (a) global view; (b) close-up view.

$$Y_3(0,\psi^*)=0.15-0.15\cos^5\left(\frac{\pi}{2}\frac{\psi^*}{2000}\right), \quad 300<\psi^*\leqslant 2000, \tag{6.13c}$$

$$\frac{\partial Y_1}{\partial \psi^*}(t^*,0)=\frac{\partial Y_1}{\partial \psi^*}(t^*,2000) =\frac{\partial Y_3}{\partial \psi^*}(t^*,0)=\frac{\partial Y_3}{\partial \psi^*}(t^*,2000)=0. \tag{6.13d}$$

The initial conditions are chosen such that the computational domain near $\psi^*=0$ has a small pocket of gas which has a composition close to that of the products at chemical equilibrium. The rest of the computational domain contains the reactant mixture. There is a reaction zone or a flame front of small initial thickness between the products and reactant mixture. After the flame front is fully developed, it propagates into the reactant mixture at a steady flame speed. The reactant mixture is at temperature $T=300$ K, hence, $h_r^*=1.432$.

Figure 8 depicts the steady state solution of the full PDEs, plotted in the two-dimensional Y_O–Y_{O_2} phase space. Stars represent the steady state solution at the actual grid points. One thousand equally spaced Lagrangian grid points were used, and for clarity every tenth grid point has been

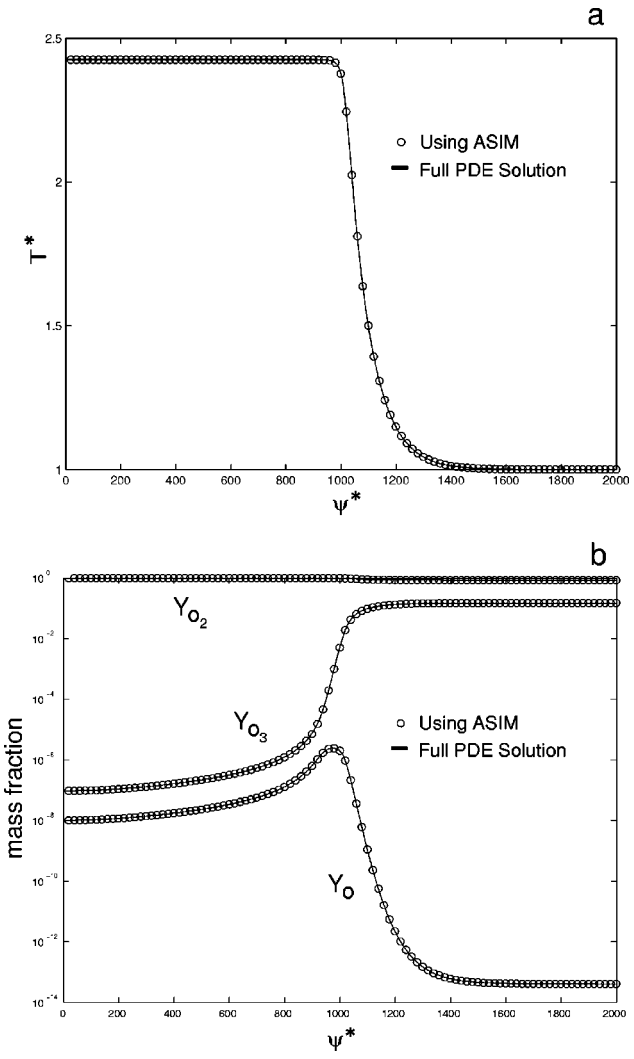

FIG. 9. Ozone decomposition flame profile at $t^* = 70\,000$ for (a) temperature, and (b) species mass fractions.

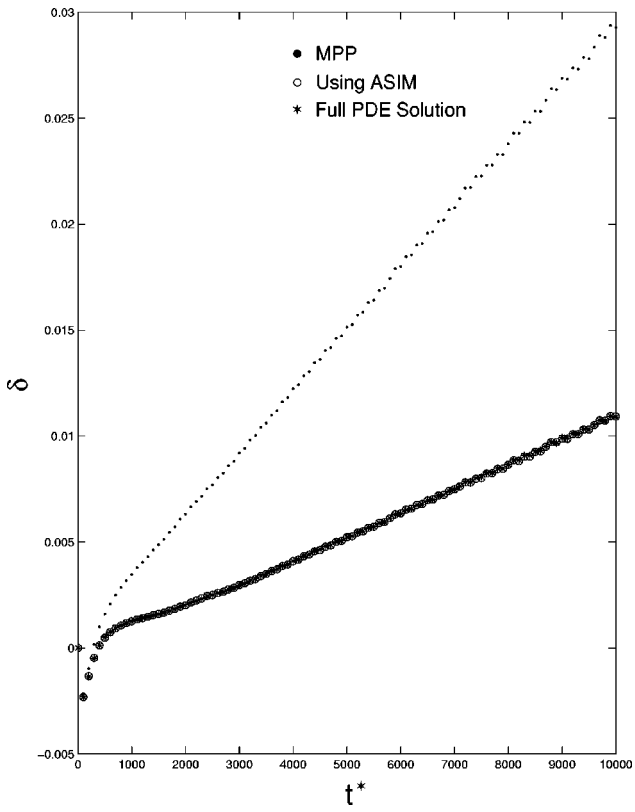

FIG. 10. The phase error δ incurred in computations of the ozone laminar flame with the three methods, at a resolution of 1000 points, relative to computations using full integration at a resolution of 10 000 points.

plotted. The numerical computations are done using second order, central difference approximations for spatial discretization and the second order BDF method in LSODE for time advancement. Also plotted is the one-dimensional ILDM as a curve in the same phase space. It can be seen from the figures that the steady solution does not lie on the ILDM. This is emphasized in Fig. 8(b) which shows a close up of the region of phase space where the difference between the steady state solution and the ILDM is maximum. Hence, forcing the solution onto the ILDM, as done in the MPP method, will lead to errors. The steady state temperature profile and mass fraction distribution of O, O_2, and O_3, in the ozone decomposition flame, are plotted in Fig. 9. The region of phase space depicted in Fig. 8(b) corresponds to the flame front in physical space. Within the flame front the temperature gradients and the mass fraction gradients are large, hence, the effects of diffusion are large. Therefore, the steady solution deviates the most from the ILDM within the flame front, as the ILDM is obtained from chemistry alone without incorporating effects of diffusion.

It can be seen from Fig. 9 that the steady profiles obtained when using the ASIM are nearly identical to those obtained by full integration. In this case, since the ASIM is given by the solution of a nonlinear boundary value problem, we have not constructed a Green's function, but instead solved a discretized form of the differential equation. However, we believe that a numerical Green's function construction procedure for solving Eq. (4.7b) may be possible.

Figure 10 compares the phase error in the solutions obtained by full integration, use of the ASIM, and the MPP method, all using a spatial resolution of 1000 grid points, relative to the baseline solution obtained by full integration at a spatial resolution of 10 000 grid points. The numerical computations are done using second order, central difference approximations for spatial discretization and the second order BDF method, in the differential algebraic solver DASSL,[43] for time advancement. Use of DASSL is not required for full integration, but it is required when using the ASIM and for the MPP method for solving the resulting differential algebraic system of equations from spatial discretization. For error analysis all the computations are done using the DASSL package with same time increments until steady state is achieved, in order to remove any numerical bias as done for the simple example in the previous section. The phase error $\boldsymbol{\delta}$ is measured as the Lagrangian distance between the location within the flame front where the mass fraction of O_3 is 0.075, for the solution obtained by the three methods and the baseline solution. We note that there is a phase difference between the full integration at 1000 grid points and the baseline solution due to the inherent phase error in the BDF numerical method used. This is depicted in

Fig. 10, where stars represent the phase error in the full integration. At steady state the flame front propagates at a uniform speed, and the phase difference increases linearly, which signifies that different flame propagation speeds or burning rates are predicted at different grid resolutions. Near steady state, as can be seen from Fig. 10, the phase errors incurred when using the ASIM and full integration with the same resolution, are essentially identical. On the other hand the phase error incurred by the MPP method is substantially larger. Hence, there is also an error in the prediction of flame propagation speed or the burning rate by the MPP method. This is evident from the difference in slopes of the phase error curve for the MPP method and the slope of the phase error curve when the ASIM or full integration is used.

We have also computed the amplitude error in the solutions obtained by the three methods relative to the baseline solution. To estimate the amplitude error the phase error has to be eliminated. This is done by first estimating the difference in the flame front propagation speeds obtained by the three methods from that of the baseline solution. The flame propagation speed can be estimated from the slope of the linear part of the phase error curves at steady state. The flame profiles are then shifted to minimize the phase error at all times. Finally, the amplitude error is estimated as the $\mathbf{L}_\infty$ norm of the error between the solution obtained by the three methods and the baseline solution. While not shown here, we find that the error incurred when using the ASIM and the error incurred by full integration is essentially identical, and both relax to a constant value of 3.75×10^{-5} at steady state. On the other hand the error in the MPP method is slightly larger (4.5×10^{-5}) and increases slowly due to the fact that the solution is forced onto the ILDM when it does not lie there.

VII. CONCLUSIONS

It has been shown that the ILDM is not a SIM, contrary to the conclusions of Rhodes *et al.*,[22] but approaches the SIM in the limit of large stiffness for spatially homogeneous reactive systems which are modeled by ODEs. While no robust analysis exists to determine convection and diffusion time scales *a priori*, we find that in reactive flow systems in which convection and diffusion have time scales comparable to those of reactions, MPP can lead to large transient and steady state errors. Thus, the error incurred when using the ASIM is much smaller than that in the MPP method. Using the ASIM, reaction, convection and diffusion can be better coupled, while systematically equilibrating fast time scales. The ASIM is shown to be a good approximation for the long time dynamics of reactive flow systems. At this point the fast and slow subspace decomposition is dependent only on reaction and should itself be modified to account for convection-diffusion effects. In this work we have illustrated the improved accuracy in describing the slow dynamics of two simple reaction-diffusion systems, when using the ASIM, with a concomitant decrease in computational cost.

ACKNOWLEDGMENTS

This work has received partial support from the National Science Foundation under CTS-9705150, the Air Force Office of Scientific Research under F49620-98-1-0206, and Los Alamos National Laboratory. The authors acknowledge useful discussions on slow manifolds with Dr. A. J. Roberts, University of Southern Queensland, Australia, as well as Dr. Christopher Bowman at the University of Notre Dame. A version of this work was first presented at the workshop on Dynamics Reduction in Chemical Kinetics, held at Argonne National Laboratory, June 2000.

[1] W. G. Vincenti and C. H. Kruger, Jr., *Introduction to Physical Gas Dynamics* (Wiley, New York, 1967).
[2] J. D. Buckmaster and G. S. S. Ludford, *Theory of Laminar Flames* (Cambridge University Press, New York, Cambridge, 1982).
[3] *Reduced Kinetic Mechanisms and Asymptotic Approximations for Methane–Air Flames: A Topical Volume*, edited by M. Smooke, with contributions from R. W. Bilger *et al.* (Springer-Verlag, Berlin, 1991).
[4] J. D. Buckmaster, Annu. Rev. Fluid Mech. **25**, 21 (1993).
[5] A. M. Khokhlov, E. S. Oran, A. Y. Chtchelkanova, and J. C. Wheeler, Combust. Flame **117**, 99 (1999).
[6] *Reduced Kinetic Mechanisms for Applications in Combustion Systems*, Lecture Notes in Physics, Vol. 15, edited by N. Peters and B. Rogg (Springer-Verlag, Berlin, 1993).
[7] J. Warnatz, U. Maas, and R. W. Dibble, *Combustion* (Springer, Berlin, 1996).
[8] U. Maas and S. B. Pope, Combust. Flame **88**, 239 (1992).
[9] G. Li and H. Rabitz, Chem. Eng. Sci. **51**, 4801 (1996).
[10] O. Gautier and R. W. Carr, Jr., Int. J. Chem. Kinet. **17**, 1347 (1985).
[11] L. Petzold and W. Zhu, AIChE J. **45**, 869 (1999).
[12] A. R. Sirdeshpande, M. G. Ierapetritou, and I. P. Androulakis, AIChE J. **47**, 2461 (2001).
[13] J. F. Griffiths, Prog. Energy Combust. Sci. **21**, 25 (1995).
[14] M. S. Okino and M. L. Mavrovouinotis, Chem. Rev. **98**, 391 (1998).
[15] S. H. Lam and D. A. Goussis, *22nd International Symposium on Combustion* (Combustion Institute, Pittsburgh, 1988), p. 931.
[16] S. H. Lam, Combust. Sci. Technol. **89**, 375 (1993).
[17] U. Maas and S. B. Pope, *24th International Symposium on Combustion* (Combustion Institute, Pittsburgh, 1992), p. 103.
[18] T. Blasenbrey, D. Schmidt, and U. Maas, *27th International Symposium on Combustion* (Combustion Institute, Pittsburgh, 1997), p. 505.
[19] R. L. G. M. Eggels, J. J. J. Louis, J. B. W. Kok, and L. P. H. DeGoey, Combust. Sci. Technol. **123**, 347 (1997).
[20] D. Schmidt, J. Segatz, U. Riedel, J. Warnatz, and U. Maas, Combust. Sci. Technol. **114**, 3 (1996).
[21] B. Yang and S. B. Pope, Combust. Flame **112**, 16 (1998).
[22] C. Rhodes, M. Morari, and S. Wiggins, Chaos **9**, 108 (1999).
[23] R. Lowe and A. Tomlin, Atmos. Environ. **34**, 2425 (2000).
[24] O. Gicquel, D. Thevenin, M. Hilka, and N. Darabiha, Combust. Theory Modell. **3**, 479 (1999).
[25] C. Correa, H. Niemann, B. Schramm, J. Warnatz, J. W. Daily, and B. Zamuner, *28th International Symposium on Combustion* (Combustion Institute, Pittsburgh, 2000), p. 1607.
[26] H. G. Kaper and T. J. Kaper, "Asymptotic analysis of two reduction methods for systems of chemical reactions" (preprint).
[27] S. J. Fraser, J. Chem. Phys. **88**, 4732 (1988).
[28] M. R. Roussel and S. J. Fraser, J. Chem. Phys. **94**, 7106 (1991).
[29] M. J. Davis and R. T. Skodje, J. Chem. Phys. **111**, 859 (1999).
[30] M. Hadjinicolaou and D. A. Goussis, SIAM J. Sci. Comput. (USA) **20**, 781 (1999).
[31] A. N. Yannacopoulos, A. S. Tomlin, J. Brindley, J. H. Merkin, and M. J. Pilling, Physica D **83**, 421 (1995).
[32] U. Maas and S. B. Pope, *25th International Symposium on Combustion* (Combustion Institute, Pittsburgh, 1994), p. 1349.

[33] G. Strang, SIAM (Soc. Ind. Appl. Math.) J. Numer. Anal. **5**, 506 (1968).
[34] S. Singh, Y. Rastigejev, S. Paolucci, and J. M. Powers, Combust. Theory Modell. **5**, 163 (2001).
[35] R. J. LeVeque and H. C. Yee, J. Comput. Phys. **86**, 187 (1990).
[36] Y. Zeldovich, J. Phys. Chem. **11**, 685 (1936).
[37] J. Carr and R. G. Muncaster, J. Diff. Eqns. **50**, 260 (1983).
[38] U. Maas, Comput. Visual. Sci. **1**, 69 (1998).
[39] M. R. Roussel, J. Math. Chem. **21**, 385 (1997).
[40] M. R. Roussel and S. J. Fraser, Chaos **11**, 196 (2001).
[41] A. C. Hindmarsh, in *Scientific Computing*, edited by R. S. Stepleman *et al.* (North–Holland, Amsterdam, 1983), p. 55.
[42] S. B. Margolis, J. Comput. Phys. **27**, 410 (1978).
[43] L. R. Petzold, in *Scientific Computing*, edited by R. S. Stepleman *et al.* (North–Holland, Amsterdam, 1983), p. 65.